

Chapter 7

Spaceborne Thermal Infrared Observation – An Overview of Most Frequently Used Sensors for Applied Research

Claudia Kuenzer, Huadong Guo, Marco Ottinger, Jianzhong Zhang,
and Stefan Dech

Abstract This chapter presents an overview of the most commonly used spaceborne sensors for thermal infrared research applications. There is a large fleet of international sensors available which allow for the acquisition of data in the thermal infrared. Depending on spatial coverage, some sensors are more suitable for mapping large areas, while others support observations at a local scale. Temporal resolution defines whether temperature patterns or phenomena can be monitored on a daily, weekly, monthly, or even only an annual basis. A wide variety of thermal sensors will be introduced in overview tables. However, as certain sensors with thermal infrared bands have established themselves as ‘work horses’ for certain types of applications, they will be especially highlighted and presented in depth. A comprehensive overview of typical thermal infrared application studies and the sensors particularly favored rounds off this chapter.

7.1 Introduction

Thermal remote sensing over land and ocean has always been a discipline with a relatively small analyst and user community compared to the fields of multispectral remote sensing or even radar remote sensing (see Table 7.1). Typical applications for thermal remote sensing over land are: large scale land surface temperature (LST) mapping for model input in the fields of vegetation monitoring, agriculture,

C. Kuenzer (✉) • M. Ottinger • S. Dech
German Remote Sensing Data Center (DFD), Earth Observation Center (EOC),
German Aerospace Center (DLR), Oberpfaffenhofen, Germany
e-mail: Claudia.kuenzer@dlr.de

H. Guo
Center for Earth Observation and Digital Earth (CEODE), Beijing, China

J. Zhang
Beijing ESKY Technology Limited, Beijing, China

Table 7.1 Number of publications related to thermal infrared research in four selected remote sensing journals in the years 2009, 2010, and 2011, with respect to the overall number of publications and different fields of application

Topic	Journals													
	International Journal of Remote Sensing				Remote Sensing of Environment				International Journal of Applied Earth Observation and Geoinformation				IEEE Transactions on Geoscience and Remote Sensing	
	2009	2010	2011	2009	2010	2011	2009	2010	2011	2009	2010	2011	2009	2011
All articles	387	387	523	255	256	330	56	91	106	374	383	424		
Thermal articles	21 (5 %)	17 (4 %)	23 (4 %)	36 (14 %)	36 (14 %)	50 (15 %)	7 (16 %)	9 (10 %)	14 (13 %)	11 (3 %)	12 (3 %)	13 (3 %)		
LST retrieval	1	–	3	4	1	4	–	–	2	2	2	4		
SST retrieval	1	3	1	3	5	5	–	–	–	–	–	–		
Urban climatology, UHI	2	–	1	2	3	4	1	1	1	–	–	–		
Other climatology	2	2	–	–	2	7	1	1	1	1	–	2		
Clouds, snow and ice	1	2	2	2	5	1	–	–	1	1	–	–		
Agriculture modeling	3	–	–	–	4	4	1	–	1	–	–	–		
Volcano analyses	–	1	1	2	1	1	–	–	–	1	1	–		
Earthquake analyses	–	1	–	–	–	–	1	1	–	–	–	–		
Geothermal research	1	–	1	–	–	–	–	–	1	–	–	–		
Forest fire analyses	2	2	2	6	4	6	1	1	1	–	–	–		
Peat fire detection	–	–	1	–	–	–	–	–	–	–	–	–		
Coal fire analyses	–	1	–	–	–	–	–	–	–	–	–	–		
Soil moisture	–	–	–	1	2	–	–	1	1	–	1	1		
Mineral discrimination	–	–	1	1	–	1	–	–	–	–	–	–		
Land cover	–	–	1	2	–	–	–	–	–	–	–	–		
Emissivity and inertia	–	–	–	3	2	1	–	1	1	–	–	–		

climatology and hydrology; analysis of thermal heat island and heat sink patterns in urban areas; urban area climatology; volcano monitoring; geothermal analysis; forest fire, peat fire, and burned area detection; observation of industrial areas, investigation of coal fire and mining areas worldwide; security applications such as pipeline monitoring; the retrieval of soil moisture data; and rock type and mineral discrimination. In the field of ocean or water surface observation, water temperature patterns, water mixing, and freeze-thaw processes are of special interest to the community focusing on sea surface temperature (SST). Despite the limited number of scientists engaged in thermal infrared (TIR) remote sensing and (compared to optical, multispectral or radar sensors) a relatively narrow choice of really suitable spaceborne thermal sensors, the applications listed above still indicate a large potential for quantitative analysis and product generation, which should not be underestimated. This chapter presents an overview of the currently available sensors with bands in the thermal infrared which are most commonly used for thermal earth observation applications.

Table 7.1 presents the number of publications related to thermal infrared research in four selected remote sensing journals for the years 2009, 2010, and 2011, with respect to the overall number of publications and sorted according to different fields of application. We can see that with respect to LST analysis, especially the application fields of general LST retrieval over land, forest fire analysis, cloud/snow/ice detection, and image classification and accuracy mapping are well represented. The latter fields are especially strong as many scientists publish work demonstrating that the inclusion of the thermal band can improve the distinction of land cover and land use classes and can therefore positively influence classification accuracy. Other field such a geothermal analyses, coal and peat fire investigations, or geo-health – to give only three examples – are less extensively dealt with. However, one has to keep in mind that in certain fields, thermal-infrared-related research findings are not published in typical remote sensing journals, but in those of other disciplines (energy, geology, environment, etc.) (ESA 2012).

7.2 Thermal Infrared Sensors

Table 7.2 gives a detailed overview of typical sensors and their characteristics (spatial resolution, revisit time, swath width, platform, agency operating the sensor and launch year) employed for the analysis of land and sea surface temperatures and related applications. Currently, most instruments stem from the USA. However, Europe also had and has several suitable sensors in space, and the upcoming Sentinel 3 satellite will have on board a thermal sensor named ‘Sea and Land Surface Temperature Radiometer’, SLSTR, providing 1 km resolution. Also, China’s fleet of spaceborne sensors, including those with thermal infrared bands, has expanded rapidly in recent years. All sensors presented are operational (unless indicated otherwise, marked grey) and deliver data.

Table 7.2 Selected sensors often used for the analysis of land surface temperature and related applications

Sensor	Spatial res.	Revisit	Swath width	Platform/satellite	Agency	Launch year
ETM+	60 m	16 d	185 km	Landsat-7	USGS, NASA	1999
TM	120 m	16 d	185 km	Landsat 5	USGS, NASA	1984
TIRS	100 m	16 d	185 km	Landsat 8 (LDCM)	USGS, NASA	2013
ASTER	90 m	4–16 d	60 km	Terra	NASA	1999
IRMSS	160 m	26 d	120 km	CBERS-1, 2, 2b	CRESDA, INPE	1999–2003, 2003, 2007–2010
IRSCAM	80 m	26 d	120 km	CBERS-3 and 4, 4b	CRESDA, INPE	2012, 2014, 2016
MERSI	250 m	1 d	2800 km	FY-3A, FY-3B	NRSCC, CAST, NSM a.o.	2008, 2010
InfraredCam	300 m	31 d	720 km	HJ-1B	CRESDA, CAST, NRSCC	2008
NIRST	351 m	< 1–2 d	182–1,060 km	Aquarius	NASA, CONAE	2011
BIRD	370 m	10 d	190 km	BIRD	DLR	2001–2004
TET-1	356 m	10 d	180 km	TET-1	DLR	2012
VIIRS	1.6 km	< 1 d	3,000 km	Suomi NPP	NASA/NOAA	2011
ChS	14 km	< 1 d	2,200 km	Suomi NPP	NASA/NOAA	2011
CERES	20 km	< 1 d	3,000 km	Suomi NPP	NASA/NOAA	2011
IIR	1 km	16 d	64 km	CALIPSO	CNES	2006
MODIS	1 km	4 per day	2,330 km	Terra, Aqua	NASA	1999, 2002
ATSR-2	1 km	3 d	512 km	ERS-2	ESA, UKSA, CSIRO	1995–2011
AATSR	1 km	35 d	500 km	Envisat	ESA, UKSA	2002–2012
AVHRR/1	1.1 km	< 1 d	2,600 km	TIROS-N, NOAA 6,8,10	NOAA	1978–1986
AVHRR/2	1.1 km	< 1 d	3,000 km	NOAA9,10,11,12,13,14	NOAA	1984–2005
AVHRR/3	1.1 km	< 1 d	3,000 km	NOAA15–19, Metop A,B	NOAA, EUMETSAT	1998, 2000, 2002, 2005, 2006, 2012

MSG-SEVIRI	1–3 km	< 1 d	Full earth disk	Meteosat-8/9/19	ESA/EUMETSAT	2002, 2005, 2012
MVIRI	5 km	ev. 30 min	Full earth disk	Meteosat-3/4/5/6/7	EUMETSAT, ESA	1988, 1989, 1991, 1993, 1997
MSU-MR	1 km	37 d	3,000 km	Meteor 3 M, and -M N1	ROSHYDROMET a.o.	2001, 2009
MSU-GS	4 km	geost. < 1 d	Full earth disk	Elektro-L N1	ROSHYDROMET a.o.	2011
IMAGER	4 km	geost., < 1 d	Full earth disk	MTSAT-1,2,3	JMA	1999, 2006, 2013
MVISR	1.1 km	3–4 d	3,200 km	FY-1C, 1D	CMA, NRSCC	1999, 2002
IVISSR	5 km	1 d	Full earth disk	FY-2C, 2D, 2E, 2 F	NRSCC, CAST, NSMC	2004, 2006, 2008, 2012
VHRR	8 km	ev. 30 min	Full earth disk	Insat-2A,B,E, -3A	ISRO	1992, 1993, 1999, 2003
IASI	25 km	29 d	2,052 km	MetOP-A/B	CNES, EUMETSAT	2006, 2012
HIRS/3	20.3 km	< 1 d	2,240 km	NOAA 15,16,17	NOAA	1998, 2000, 2002
HIRS/4	20.3 km	< 1 d	2,240 km	NOAA 18/19, MetOp A/B	NOAA, EUMETSAT	2005, 2006, 2009, 2012
ScaRaB	40 km	1 d	2,200 km	Meteor-3, Resurs-01, Megha Tropiques	CNES	1994, 1998, 2011

Spatial resolution is presented for the commonly used TIR domain above 8 μm
 Agency Code for Table 7.2: USA: NASA National Aeronautics and Space Administration, *USGS* United States Geological Survey, *NOAA* National Oceanic and Atmospheric Administration, Europe: *ESA* European Space Agency, *EUMETSAT* European Organization for the Exploitation of Meteorological Satellites, *UKSA* UK Space Agency, *DLR* German Aerospace Center, *CNES* Centre National d'Etudes Spatiales, China: *CRESDA* China Centre for Resources Satellite Data and Application, *CMA* Chinese Meteorological Administration, *NRSCC* National Remote Sensing Center China, *CNSA* Chinese National Space Administration, *CAST* Chinese Academy of Science and Technology, Japan: *JAXA* Japan Aerospace Exploration Agency, *JMA* Japan Meteorological Administration, India: *ISRO* Indian Space Research Organisation, Australia: *CSIRO* Commonwealth Scientific and Industrial Research Organisation. *a.o.* amongst others

7.2.1 Overview of Selected Sensors with Thermal Infrared Instruments

The following list presents the full names of sensors listed in Table 7.2.

- ETM+: Enhanced Thematic Mapper (on board the U.S. Landsat 7)
- TM: Thematic Mapper (on board the U.S. Landsat 5)
- TIRS: Thermal InfraRed Sensor (on board the U.S. Landsat DCM)
- ASTER: Advanced Spaceborne Thermal Emission & Reflection Radiometer (on board the American-Japanese sensor of the same name, on the Terra platform)
- IRMSS: InfraRed MultiSpectral Sensor (on board the Chinese CBERS 1, 2, and 2b)
- IRSCAM: Infrared Medium Resolution Camera (on board the Chinese CBERS 3, and future CBERS 4 and 4b)
- InfraredCamera (on board the Chinese HJ-1B satellite)
- MERSI: Medium Resolution Spectral Imager (on board the Chinese FengYun satellites)
- NIRST: New Infrared Sensor Technology (on board the American Aquarius)
- BIRD: Bi-spectral Infrared Detection (on board the German sensor of the same name)
- TET: Technologie Entwicklungsträger (on board the German sensor of the same name)
- VIIRS: Visible/Infrared Imager Radiometer Suite (on board the U.S. Suomi NPP)
- CrIS: Cross-track Infrared Sounder (on board the U.S. Suomi NPP)
- CERES: Cloud's and Earth's Radiant Energy System (on board the U.S. Suomi NPP)
- IIR: Imaging Infrared Radiometer (on board the French CALIPSO satellite)
- MODIS: Moderate Resolution Imaging Spectroradiometer (on the U.S. platforms Terra and Aqua)
- AATSR: Advanced Along-Track Scanning Radiometer (on board the European Envisat)
- AVHRR: Advanced Very High Resolution Radiometer (on board the U.S. NOAA satellites)
- MSG-SEVIRI: Meteosat Second Generation – Spinning Enhanced Visible and InfraRed Imager (on board the European METEOSAT Second Generation satellites)
- MVIRI: Meteosat Visible and InfraRed Imager (on board the geostationary European METEOSAT satellites)
- MSU-MR: Multispectral scanning imager-radiometer (on board the Russian orbiting Meteor-M N1 meteorological satellite)
- MSU-GS: Multispectral scanning imager-radiometer (on board the Russian geostationary Elektro-L N1 meteorological satellite)

- Imager: Multiband Imager (on board the MTSAT Japanese meteorological satellites)
- MVISR: Multispectral Visible and Infra-red Scan Radiometer (on board the Chinese FengYun meteorological satellites)
- IVISSR: Improved Multispectral Visible and Infra-red Scan Radiometer (on board the operating Chinese FengYun meteorological satellites)
- VHRR: Very High Resolution Radiometer (on board the Indian National Satellite System INSAT)
- IASI: Infrared Atmospheric Sounding Interferometer (on board the European Metop-A, Metop-B satellites)
- HIRS: High Resolution Infrared Radiation Sounder (in different versions as HIRS/2/3/4 on board the U.S. NOAA and European Metop series)
- ScaRaB: Scanner for Earth's Radiation Budget (on board the French satellite Megha Tropiques)

In Table 7.2 some sensors or satellites are marked in grey. These are no longer operational, but they are listed here as they were extensively used by the thermal infrared community, and as we want to indicate the availability of the relevant data archives for long term monitoring purposes. Concerning spatial resolution, the pixel resolution in the TIR band(s) (usually located somewhere in the 8–14 μm domain) is given. Furthermore, we elaborate on some of the thermal instruments in detail. Here we selected the most commonly employed satellites such as Landsat-7, ASTER, CBERS, HJ-1B, MODIS, and AVHRR/3. These (amongst other) have been – or are currently – widely used in the application studies presented in SCI journals.

7.2.2 Landsat-7 ETM+ Thermal Infrared Data

The Landsat ETM+ characteristics were already briefly introduced in Chap. 1 of this book. However, as Landsat-7 ETM+ has been – for many years – a work horse for the thermal infrared community, and as this chapter might be read independently of the remaining chapters of this book, some facts are repeated here. The new Landsat DCM (Data Continuity Mission) sensor is covered in a separate chapter of this book. The ETM+ sensor has one thermal band in the 10.4–12.5 μm domain delivering data at a spatial resolution of 60 m. For ETM+ all bands are acquired in either a low- or high-gain mode. Gain selection is defined in the gain strategy of the former Long Term Acquisition Plan (LTAP), depending on acquisition time and the dominant surface types in a scene (percentages of land, desert, ice/snow, water, sea ice, etc.). These are known a priori, based on maps. Except for very specific requests the user has no influence on the gain setting in the reflective modes. Nevertheless, LS-7 band 6 will always be recorded and delivered in the low-gain and high-gain mode. These double gain settings extend the temperature range. However, detector saturation can occur if a surface has extremely high temperatures, or – vice versa – a surface will not be

Table 7.3 Temperature of saturation in the low- and high-gain bands of Landsat-7 ETM+ with an 8 bit dynamic range

Part of the EMS	Band width/EMR-area [μm]	Minimum temperature [$^{\circ}\text{C}$]	Maximum temperature [$^{\circ}\text{C}$]
1 (VIS, blue)	0.45–0.51	1,051 (1,075)	1,483 (1,526)
2 (VIS, green)	0.52–0.60	900 (922)	1,301 (1,340)
3 (VIS, red)	0.63–0.69	755 (775)	1,119 (1,156)
4 (NIR)	0.75–0.90	595 (613)	926 (961)
5 (SWIR)	1.55–1.75	206 (217)	417 (440)
6 (TIR)	10.40–12.50	–33 (–134)	51 (77)
7 (SWIR)	2.09–2.35	92 (101)	258 (276)
8 (PAN)	0.52–0.90	702 (721)	1,056 (1,092)

Source: Flynn et al. (2001), modified

detected thermally if its temperature is below a certain threshold. Table 7.3 lists the minimum and maximum temperatures in the low-gain and high-gain setting, indicating the lowest or highest pixel integrated temperature which can be detected in a certain wavelength region. It also shows that the mid-infrared band 5 can be used to detect thermal anomalies of very high temperatures leading to saturation in band 6. Even the near-infrared channel 4 offers options for the detection of extremely high temperatures.

Although the low-and high-gain options are new compared to the former Landsat-TM, the thermal bands of ETM+ are less suitable for high temperature studies. They saturate at 51 and 77 $^{\circ}\text{C}$, respectively, while TM band 6 saturates at around 90 $^{\circ}\text{C}$. It is also often stated that ETM+ still suffers from an antiquated 8 bit dynamic range, limiting radiance steps to 256 instead of, e.g., 4,096 if a 12 bit system is used (Flynn et al. 2001). However, the major difference to ETM+ data is the lower spatial resolution in the thermal band (120 m, no double gain setting) and the lack of a panchromatic channel for the visible domain. Furthermore, Landsat TM data have a weaker SNR ratio and radiometric sensitivity. However, Landsat-5 TM is still acquiring up-to-date images of the earth's surface and provides an important data source for many thermal applications.

Figure 7.1 presents a subset of a multispectral combination and a thermal band of Landsat-7 ETM+ acquired over the Wuda coal mining area in Inner Mongolia, China. The Yellow River in the center of the subset runs from south to north. It is frozen in most parts and temperatures range between -2 to 1 $^{\circ}\text{C}$. Coal surfaces (which can be recognized as black spots in the 'ear-shaped' coal mining syncline west of the river, as well as in some locations in the south-eastern quarter of the subset) and sun-exposed geologic surfaces are the warmest areas (15 – 29 $^{\circ}\text{C}$), while the deeply incised valleys on the eastern side of the Yellow River and the northwest exposed slopes in the northern Helan Mountains in the southwestern quarter are the coldest regions (-13 to 0 $^{\circ}\text{C}$). When radiometrically correcting winter scenes it has to be taken into account that negative temperature values may occur, and therefore the data has to be handled as "signed" bit instead of "unsigned" bit data; otherwise all negative temperatures will appear as 0 $^{\circ}\text{C}$.

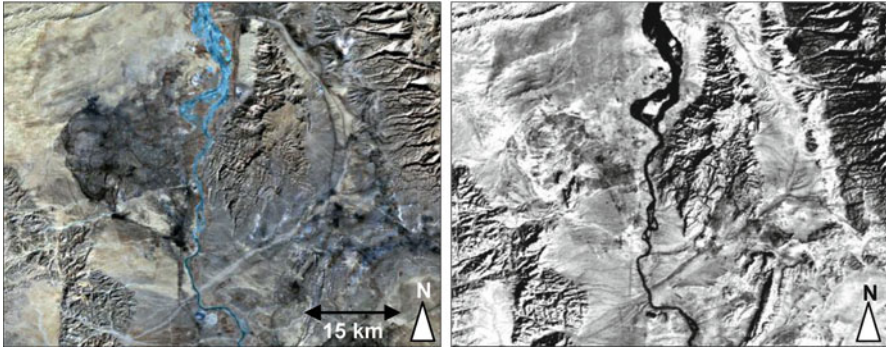


Fig. 7.1 Subset of a multispectral and a thermal daytime scene acquired by Landsat-7 ETM+ on 12.02.2003, 2 months before the scan mirror failure. *Left:* false color infrared image, *right:* DNs converted to temperature in °C. *Light:* high temperatures, *dark:* lower temperatures. Temperature range: -13 to 29 °C. Center location: 650695E, 4373295N, UTM, Z48N

Upon special request it is possible to plan specific nighttime acquisitions of Landsat (thermal only). The scheduling of nighttime acquisition is usually only possible for selected projects and users. Only a limited amount of nighttime data can be acquired during a satellite's path around the world, since acquisition on the nighttime side (descending orbit) requires more energy than a daytime acquisition. The acquisition of one nighttime scene will lead to the skipping of seven daytime frames in the ascending daytime orbit. However, nighttime data acquired in the past is usually available in the worldwide data archives and can be ordered by every user.

ETM+ thermal data has been available since 1999. In May 2003 the ETM+ sensor had a technical failure in a scan mirror. However, according to the Landsat science team 78 % of the data sets are unaffected and can be ordered. However, many scientists have stopped using ETM+ instead of analyzing whether the scan mirror problem even affects their area of interest or the data quality for their purposes. The new sensor Landsat Data Continuity Mission, LDCM, with its TIRS instrument acquiring data in the thermal domain, is presented in its own chapter in this book. Unfortunately, the thermal infrared band comes at a spatial resolution of 100 m, which is lower than the 60 m resolved thermal band of the foregoing ETM+ sensor.

7.2.3 ASTER Thermal Infrared Data

The spectral and spatial properties of the ASTER sensor, installed on the Terra platform and flying 30 min behind Landsat-7, are briefly introduced in Table 7.4. Since December 1999 ASTER has traveled in a near polar, sun synchronous orbit, acquiring data since February 24, 2000 with a repetition rate of 16 days. Data is down-linked in frames covering an area of approximately 60 km × 60 km at

Table 7.4 Spectral and spatial properties of ASTER data

Part of the electromagnetic spectrum	Band width/EMR-area [μm]	Spatial resolution [m]	Depth [bit]
(1) VNIR	0.52–0.60	15	8
(2) VNIR	0.63–0.69	15	8
(3) VNIR nadir looking	0.76–0.86	15	8
(3) VNIR backward looking	0.76–0.86	15	8
(4) SWIR	1.6–1.7	15	8
(5) SWIR	2.145–2.185	30	8
(6) SWIR	2.185–2.225	30	8
(7) SWIR	2.235–2.285	30	8
(8) SWIR	2.295–2.365	30	8
(9) SWIR	2.360–2.430	30	8
(11) TIR	8.125–8.475	90	12
(12) TIR	8.475–8.825	90	12
(13) TIR	8.925–9.275	90	12
(14) TIR	10.25–10.95	90	12
(15) TIR	10.95–11.65	90	12

10:30 a.m. local time. Unlike Landsat-7, which acquires (acquired) data constantly and therefore provided near-worldwide coverage of frames (except the poles), ASTER only scans the earth's surface when specifically requested by a customer. Thus it does not grant sufficient areal coverage (Earth Remote Sensing Data Analysis Center. 2000, 2001; Abrams and Hook 1995). Nighttime data with five thermal bands, acquired at 10:30 p.m. local time, can also be requested by users. A major advantage of such thermal nighttime data is that at that time only a few solar effects modify the thermal signal. Influences of uneven heating due to slope and aspect are minimized (Kuenzer 2005; Zhang and Kuenzer 2007; Zhang et al. 2007). However, the optimal time for thermal data acquisition would be around 5 a.m., shortly before sunrise, when objects on the earth's surface have the lowest temperature and the solar effect is least accentuated (Zhang and Kuenzer 2007).

A large advantage and unique feature of the ASTER sensor is the availability of five bands in the TIR between 8.125 and 11.65 μm at 90 m spatial resolution at a 12 bit dynamic range. Even MODIS has only two bands in the TIR domain and only at 1 km resolution. ASTER therefore allows discrete emissivity-influenced spectra of surfaces to be mapped based on five measurements. As elaborated in Chap. 1, emissivity of a surface varies depending on wavelength. Therefore, an object with a certain kinetic temperature depicts different amounts of emitted radiation at different wavelengths in the thermal domain. If thorough atmospheric correction and emissivity normalization is performed, it is possible to utilize data of these five bands for emissivity-based surface mapping and surface discrimination. ASTER thermal bands are thus very widely used for mineral mapping in arid areas, as presented by Tangestani et al. (2005), Mars and Rowan (2006), and Pour and Hashim (2012), amongst many others.

Table 7.5 Infrared Scanner, IRS on board CBERS-3

Part of the EMS	Band width/EMR-range [μm]	Spatial resolution	Technical characteristics
MIR	6: 0.5–0.9	40 m	8 bit
SWIR	7: 1.55–1.75	40 m	120 km swath
	8: 2.08–2.35	40 m	No side looking option
TIR	9: 10.4–12.5	80 m	

7.2.4 CBERS Thermal Infrared Data

The China-Brazil Earth Resources Satellite CBERS-1 was launched in October 1999, followed by CBERS-2 in October 2003. CBERS-1 operated from 1999 until 2003, but CBERS-2 is still delivering data with its three instruments: the Charge Coupled Device Camera (CCD), the Wide Field Imager (WFI) and the Infrared Multi-Spectral Scanner (IRMSS). The latter also includes a thermal band at 10.40–12.5 μm at 156 m resolution. CBERS-2b was launched in 2007 and operated for 3 years. CBERS-3 was launched ahead of schedule in fall 2012, and it has an improved infrared scanner on board which delivers thermal data in the 10.40–12.5 μm range covering a swath width of 120 km at now 80 m resolution. The resolution is thus better than that of the Landsat DCM thermal band. A panchromatic band at 5 m resolution, and multispectral bands at 10 m resolution are also available and cover a swath of 60 km. CBERS-4 and CBERS-4b are currently in the assembly phase and due to be launched in 2014 and 2016, respectively. CBERS is widely used by the Chinese thermal remote sensing community, amongst others purposes also to fill existing data gaps in thermal Landsat ETM+ data (Chen et al. 2011) (Table 7.5).

7.2.5 HJ-1B Thermal Infrared Data

HJ stands for HuanJing, which means “environment” in Chinese. The HJ-1B satellite belongs to a fleet of three (and in the future more) satellites which were launched in September 2006 (HJ-1A, and HJ-1B) and November 2012 (HJ-1C). The three satellites were and are mainly used for national disaster and environmental monitoring and can acquire multispectral and radar imagery. HJ-1A, which covered two bands in the TIR at 1.1 km spatial resolution, is no longer operational. However, HJ-1B has an infrared camera on board which acquires data in the thermal domain from 10.5 to 12.5 μm at 300 m spatial resolution, covering a swath of 720 km. One band in the 3.50–3.90 μm MIR domain collects data at 150 m resolution and allows for the detection of extremely hot thermal events. HJ-1B thermal data is mainly used for general LST retrieval and the analysis of LST patterns. Due to the novelty of the HJ series, thermal data from HJ-1B has furthermore extensively been compared with other spaceborne thermal data, airborne data, and in-situ calibration measurements. Publications in English SCI journals on HJ-1B thermal data utilization are still rare, which can be attributed to the novelty of the sensor, as well as the mainly national data analyses for Chinese territory.

Table 7.6 Spectral and spatial characteristics of the MODIS mid-infrared (MIR) and thermal infrared (TIR) bands suitable for thermal earth-surface analyses

Part of the EMS	Band width/ EMR-range [μm]	Spatial resolution [km]	Technical characteristics
MIR	20: 3.660–3.840	1	12 bit
	21: 3.929–3.989	1	2,330 km swath
	22: 3.929–3.989	1	FOV $\pm 55^\circ$
	23: 4.020–4.080	1	
TIR	31: 10.780–11.280	1	
	32: 11.770–12.270	1	

It should be noted that MODIS has more channels in the MIR and TIR. However, due to water absorption they are not employable for land temperature investigations

7.2.6 MODIS Thermal Infrared Data

The MODIS sensor acquires data in 36 spectral bands ranging from 0.62 to 14.385 μm . Spatial resolution at nadir is 250 m for bands 1 and 2 (VIS), 500 m for bands 3–7 (VIS and NIR) and 1,000 m for bands 8–36 (visible (VIS), near infrared (NIR), middle infrared (MIR), TIR). At the sensor's maximum scan angle of 55° near the far end of a swath the pixel sizes can reach almost 2 km * 5 km. However, large swath widths grant a higher revisiting frequency so that MODIS data is available daily for most spots on the earth's surface. Due to the installation of the sensor on the TERRA platform (launched 1999) and an identical instrument on the AQUA platform (launched 2002), most areas can be covered 4–5 times daily: in the morning, afternoon, evening, and pre-dawn. This grants frequent cloud-free observations and continuous monitoring of a desired area. For thermal research especially bands 20–23 (ranging from 3.66 to 4.08 μm) as well as bands 31 and 32 (ranging from 10.78 to 12.27 μm) are of interest. These bands were designed for land surface temperature analysis and are shown in Table 7.6.

Kuenzer et al. (2008) have demonstrated the potential of MODIS multi-diurnal thermal observation. Four observations per day allow the discrimination of clear thermal daytime versus nighttime patterns, and can even support the analysis of hot spot dynamics over the course of a 24 h cycle. The availability of several MIR and TIR bands furthermore allows for the creation of ratio images and therefore the delineation of exceptional versus 'normal' hot spots.

MODIS thermal bands data have been widely used for land surface temperature pattern analyses, sea surface temperature studies, as well as forest fire detection (see the application section).

7.2.7 NOAA-AVHRR/3 Thermal Infrared Data

The Advanced Very High Resolution Radiometer/3 (AVHRR/3), launched for the first time in 1998, consists of six channels with a spectral range from 0.58 to

Table 7.7 Spectral and spatial characteristics of the NOAA-AVHRR/3 sensor

Part of the EMS	Band width/ EMR-range [μm]	Spatial resolution [km]	Technical characteristics
VIS	1: 0.58–0.68	1.1	10 bit, 1,090 m spatial resolution at nadir, 2,900 km swath width
NIR	2: 0.725–1.00	1.1	
SWIR	3a: 1.58–1.64	1.1	
MIR	3b: 3.55–3.93	1.1	
TIR	4: 10.30–11.30	1.1	
	5: 11.50–12.50	1.1	

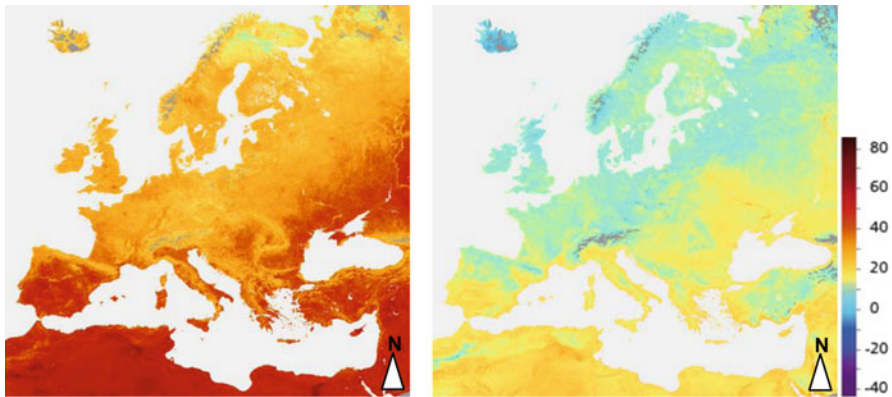


Fig. 7.2 Land surface temperature monthly composite derived from NOAA-18 AVHRR/3 data for Europe, June 2009. *Left*: daytime composite, *right*: nighttime composite. Daytime temperatures range between 10 °C in northern Norway and Finland, upto around 70° and more in northern Africa. Nighttime temperature range between 5 and 30 °C. *Grey*: no values

12.5 μm . Nadir resolution of all bands is 1.1 km. With a swath of approx. 2,900 km, it ensures full global coverage twice daily. Thermal data from AVHRR have been widely used for applications related to land surface and sea surface temperature. A large advantage of the AVHRR is its daily (actually twice daily) revisit time, and the availability of data covering the last three decades. It is therefore the only sensor in space which allows for real trend analyses (Table 7.7 and Fig. 7.2).

7.3 Selected Fields of TIR Applications and Selected Publications Sorted by Sensor

We provide below a compilation of application studies in typical application fields for thermal infrared data, sorted by field of application and most common sensors used. All references are from remote sensing SCI journals. They are not additionally included in the references section of this book chapter for reasons of space.

However, interested readers will find the respective source when searching in the Internet for the application field, sensor, and author name. For each field of application the studies are presented in a sequence from lower to higher spatial resolution TIR sensors. Please note that there is no claim of completeness, neither for the selected application fields nor the sensor lists, and that the emphasis has been placed on selecting references from the past decade.

Land surface temperature retrieval, LST

MSG SEVIRI (Stisen et al. 2007; Göttsche and Olesen 2009; Lu et al. 2011; Freitas et al. 2010; Sun and Pinker 2007; Schroedter-Homscheidt et al. 2011), **NOAA-AVHRR** (Czajkowski et al. 1998; Gleason et al. 2002; Han et al. 2004; Kerényi and Putsay 2000; Price 1983; Sobrino et al. 1994; Bhattacharya et al. 2009; Raynolds et al. 2008), **MODIS** (Petitcolin and Vermote 2002; Wan and Li 1997; Wan et al. 2002; Mito et al. 2006; Momeni and Saradjian 2007; Pinheiro et al. 2007; Agam et al. 2007; Nonaka et al. 2007; Wang et al. 2007; Song and Zhao 2007; Bhattacharya et al. 2009; Hulley and Hook 2009a; Wang and Liang 2009a; Coops et al. 2009; Vancutsem et al. 2010; Yang et al. 2011; Westermann et al. 2011; Albright et al. 2011; Hulley and Hook 2011; Wan 2008; Hashimoto et al. 2008; Wang et al. 2008; Huang et al. 2008; Mostovoy et al. 2008; McCabe et al. 2008; Langer et al. 2010), **AATSR** (Sòria and Sobrino 2007), **HJ-1B** (Zhou et al. 2010; Zhao et al. 2010; Hua et al. 2010; Xiaoguang et al. 2009), **FengYun** (Tang and Li 2012; Tang et al. 2008), **CBERS-2** (Zhang et al. 2006, Shi 2009; Yu et al. 2009), **Landsat-5 TM** (Li et al. 2004, Nichol 1998, Okwen et al. 2011; Jiménez-Muñoz et al. 2009), **Landsat 7 ETM+** (Li et al. 2004, Wloczyk et al. 2011, Okwen et al. 2011; Yue et al. 2007; Weng and Lu 2008), **ASTER** (Sobrino et al. 2007b; Mao et al. 2011; Wang and Liang 2009; Yang et al. 2011; Mira et al. 2009; Wang et al. 2011; Hulley and Hook 2011; Mao et al. 2008)

Sea surface temperature retrieval, SST

MSG SEVIRI (Clerici 2009; Merchant et al. 2009; Petrenko et al. 2011; Le Borgne et al. 2011), **NOAA-AVHRR** (Romo et al. 2007; Sousa et al. 2008; Sun et al. 2008; Chang et al. 2008; Iwasaki et al. 2008; Wang et al. 2010; Williams et al. 2010; Miliaresis and Seymour 2011; Breaker et al. 2010; Castro et al. 2010; Hulley et al. 2011; Eastwood et al. 2011), **MODIS** (Panda et al. 2007; Cai et al. 2007a; Reinart and Reinhold 2008; Cai et al. 2010; Crosman and Horel 2009; Alcantara et al. 2010; Hulley et al. 2011), **HJ-1B** (Hu et al. 2011; Huang et al. 2011; Zhou et al. 2011), **FengYun** (Wan Kadir and Rasib 2007; Zhou et al. 2008), **CBERS-2** (Wang et al. 2011), **Landsat TM/ETM+** (Isoguchi et al. 2009), **ASTER** (Sentlinger et al. 2008; Cai et al. 2010, Hulley et al. 2011; Matsuoka et al. 2011)

Clouds, snow, ice, and glaciers

MSG-SEVIRI (Mackie et al. 2010a; Mackie et al. 2010b; Pérez et al. 2011; Guo and Wang 2008; Turk et al. 2010), **NOAA-AVHRR** (Laine 2008; Turk et al. 2010; Berque et al. 2011; Fontana et al. 2009; Pérez et al. 2011), **MODIS** (Genkova et al. 2007; Stamnes et al. 2007; Aoki et al. 2007; Hori et al. 2007; Yu et al. 2007; Hall et al. 2008; Luo et al. 2008; Guo and Wang 2008; Turk et al. 2010; Fraser et al.

2010; Fraser et al. 2009), **CBERS-2** (Ribeiro et al. 2007), **Landsat** (Hall et al. 2008; Hilker et al. 2009; Helmer et al. 2010; Hagolle et al. 2010; Huang et al. 2010), **ASTER** (Genkova et al. 2007; Hall et al. 2008; Bhambri et al. 2011; Shukla et al. 2010), **Ground based TIR cameras** (Rees et al. 1993; Rees and James 1992; Leppäranta and Lewis 2007)

Climatology and evaporation

MSG-SEVIRI (Stisen et al. 2008; De Paepe et al. 2008; Sobrino and Romaguera 2008; Nieto et al. 2011; Chaurasia et al. 2010), **GOES** (Han et al. 2010; McNider et al. 1994), **FY-2** (Shu et al. 2011), **NOAA-AVHRR** (Rotach et al. 2005; Owen et al. 1998; Latifovic and Pouliot 2007; Sobrino et al. 2007a; Choudhury et al. 2007; Han et al. 2004; Han et al. 2010), **MODIS** (Cleugh et al. 2007; Rotach et al. 2005; Sánchez et al. 2007; Mallick et al. 2007; Song and Zhao 2007; Tang et al. 2010; Jang et al. 2010; Mu et al. 2011; Pouteau et al. 2011; Shu et al. 2011; Vinukollu et al. 2011; McCabe et al. 2008; Ghoneim 2008), **FengYun** (Shu et al. 2011; Shu 2010; Yun-Qiao 2011), **Landsat TM/ ETM+** (Rotach et al. 2005; Chavez et al. 2009), **ASTER** (Sarwar and Bill 2007; Nichol and Wong 2008; Bawazir et al. 2009; Galleguillos et al. 2011; Gangopadhyay et al. 2009).

Soil moisture

NOAA-AVHRR (Van den Hurk 2001; Verstraeten et al. 2006), **MODIS** (Cai et al. 2007b; Merlin et al. 2009; Hulley et al. 2010; Merlin et al. 2010; Van doninck et al. 2011), **Landsat TM** (Van den Hurk 2001), **ASTER** (Merlin et al. 2009; Hulley et al. 2010; Mira et al. 2010)

Urban climatology, heat islands

NOAA-AVHRR (Rigo et al. 2006; Gallo et al. 1993; Streutker 2003; Gallo and Owen 2002; Stathopoulou and Cartalis 2009), **MODIS** (Rigo et al. 2006; Imhoff et al. 2010; Keramitsoglou et al. 2011; Schwarz et al. 2011), **HJ-1B** (Yang et al. 2010; Luo et al. 2011), **CBERS-2** (Ji et al. 2009), **Landsat TM/ ETM+** (Rigo et al. 2006; Kim 1992; Yuan and Bauer 2007; Pena 2008; Cai et al. 2011; Amiri et al. 2009; Imhoff et al. 2010; Li et al. 2011; Zhang et al. 2009; Ma et al. 2010; Leak and Venugopal 1990; Munier and Burger, 2001), **ASTER** (Kato and Yamaguchi 2007; Frey et al. 2007; Tiangco et al. 2008; Weng et al. 2009; Cai et al. 2011; Dominguez et al. 2011; Weng et al. 2011), **Airborne TIR camera** (Lagouarde et al. 2010), **Ground based TIR cameras** (Rigo et al. 2006; Meier et al. 2010)

Agriculture modeling

NOAA-AVHRR (Hurtado et al. 1994; Salazar et al. 2008; Biradar et al. 2009), **MODIS** (Jonna et al. 2007; Sims et al. 2008; Merlin et al. 2010; Tang et al. 2010; Jeganathan et al. 2011), **HJ-1B** (Klaasse and Jarmain 2011), **ASTER** (Sepulcre-Canto et al. 2007; Courault et al. 2009; Merlin et al. 2010; Jeganathan et al. 2011), **Airborne Camera** (Suárez et al. 2010)

Forest fire detection and burnt area delineation

MSG-SEVIRI (Roberts et al. 2011; Amraoui et al. 2010; Freeborn 2009; Calle et al. 2009), **NOAA-AVHRR** (Galindo et al. 2003; Kucera et al. 2005; Smith et al.

2007; Leblon et al. 2007; Ressler et al. 2009), **MODIS** (Kazi et al. 2006; Kiran Chand et al. 2006; Morissette et al. 2005; Mazzoni et al. 2007; Smith et al. 2007; Koltunov and Ustin 2007; Kiran Chand et al. 2007; Miettinen and Liew 2008; Bromley 2010; Quintano et al. 2010; He and Li 2011; Giglio et al. 2009; Ressler et al. 2009; Freeborn 2009; Libonati et al. 2010; Libonati et al. 2011; Veraverbeke et al. 2011; Dennison and Matheson 2011; Roberts et al. 2011; Freeborn et al. 2011; Siljander 2009), **BIRD** (Oertel et al. 2003; Oertel et al. 2004), **HJ-1B** (Qian et al. 2009; Yonggang et al. 2008), **FengYun** (Zhang et al. 2011; Frantzova et al. 2010), **CBERS-2** (Zhang et al. 2011), **Landsat TM/ ETM+** (Schroeder et al. 2008), **ASTER** (Morissette et al. 2005; Schroeder et al. 2008; Giglio et al. 2008; Eckmann et al. 2009; Dennison and Matheson 2011; Veraverbeke et al. 2011), **Airborne Camera** (Riccio et al. 2011)

Coal and peat fire detection and analysis

NOAA-AVHRR (Mansor et al. 1994; Zhang et al. 2004), **MODIS** (Kuenzer et al. 2007; Kuenzer et al. 2008), **BIRD** (Siegert et al. 2004), **Landsat TM/ ETM+** (Kuenzer et al. 2007; Kuenzer 2005; Zhang et al. 2004a; Chen et al. 2007; Martha et al. 2010), **ASTER** (Kuenzer et al. 2007; Martha et al. 2010), **Ground measurements** (Zhang and Kuenzer 2007; Yunhao et al. 2007; Zhang et al. 2004; Prakash et al. 1999)

Volcano analysis

MSG-SEVIRI (Hirn et al. 2009), **NOAA-AVHRR** (Van Manen et al. 2011; Marchese et al. 2011), **MODIS** (Thomas et al. 2009), **Landsat TM/ EM+** (Deroin et al. 1995; Ganas and Lagios 2003), **SPOT** (Deroin et al. 1995), **ASTER** (Ganas et al. 2010; Carter and Ramsey 2009), **Ground based TIR camera** (Corradini et al. 2010)

Earthquake (precursor) analysis

NOAA-AVHRR (Saraf et al. 2009), **MODIS** (Saraf et al. 2009), **ASTER** (Yang et al. 2010), **Landsat ETM+** (Yang et al. 2010), **MTSAT** (Yang and Guo 2010)

Land cover discrimination

MSG-SEVIRI (Fensholt et al. 2011), **MODIS** (French and Inamdar 2010), **Landsat TM/ ETM+** (Xian et al. 2009; Fernández et al. 2010; Xian and Homer 2010; Roy et al. 2010; Wu et al. 2010; Southworth 2004).

Rock type/mineral discrimination

MSG-SEVIRI (Li et al. 2007; Klüser and Schepanski 2009), **ASTER** (Ninomiya et al. 1997; Katra and Lancaster 2008; Moore et al. 2008; Öztan and Sützen 2011; Vicente and Souza Filho 2011), **Ground based TIR camera** (Wu et al. 2011)

Emissivity and inertia studies

NOAA-AVHRR (Cracknell and Xue 1996a; Cracknell and Xue 1996b; Badenas 1998; Stathopoulou et al. 2007), **MODIS** (Nicolòs et al. 2007; Pipunic et al. 2008; Renzullo et al. 2008; Tang and Li 2008), **HJ-1B** (ShanShan et al. 2012), **FengYun** (Jiang and Zhou 2011), **ASTER** (Gangopadhyay et al. 2005; Coll et al. 2007; Hulley and Hook 2009b; Hulley et al. 2009; Sabol et al. 2009).

Accuracy assessments/Sensor calibration

MSG-SEVIRI (Nicolòs et al. 2011; Baraldi et al. 2010), **ASTER** (Gillespie et al. 2011; Yang et al. 2010; Mira et al. 2011), **NOAA-AVHRR** (Devasthale and Grassl 2009; Casciello et al. 2011; Baraldi et al. 2010), **MODIS** (Hao and Qu 2009; Wang and Liang 2009b; Chander et al. 2010; Xiaoxiong et al. 2009a; Xiaoxiong et al. 2009b); **AATSR** (Shi 2011; Baraldi et al. 2010), **HJ-1B** (Du et al. 2011), **FengYun** (Tong et al. 2010; Xiuqing et al. 2001), **CBERS-2** (Zhang et al. 2005; Zhang et al. 2002), **Landsat** (Jing and Cheng 2010; Chander et al. 2009; Chander et al. 2010; Wulder et al. 2011; Baraldi et al. 2010), **Airborne camera** (Houborg et al. 2011)

Vegetation/Forest

NOAA-AVHRR (Bhuiyan and Kogan 2010; Julien and Sobrino 2009), **MODIS** (Wu et al. 2010; Waring et al. 2011; Xu et al. 2011), **Landsat** (Potapov et al. 2011), **Airborne camera** (Zarco-Tejada et al. 2009; Ribeiro da Luz and Crowley 2010; Berni et al. 2009b)

Atmospheric correction

MODIS (Jiménez-Muñoz et al. 2010; Ellicot et al. 2009), **Landsat ETM+** (Coll et al. 2010), **ASTER** (Chrysoulakis et al. 2010).

Drought events

NOAA-AVHRR (Shamsipour et al. 2011), **MODIS** (Caccamo et al. 2011), **FengYun** (Frantzova et al. 2010), **Landsat TM/ ETM+** (Gao et al. 2011).

7.4 Conclusion

A large variety of instruments acquiring data in the thermal infrared domain (TIR) exist. They span a broad range: from sensors acquiring data for the whole earth disk at a temporal resolution allowing daily or even hourly observations at low spatial resolutions of several tenths of kilometers to one kilometer up to sensors delivering thermal data with a spatial resolution of up to 60 m at swath widths well below 200 km and repetition rates enabling only one to two observations per month. Sensors of high value for long term observation allowing a look into the past for up to nearly 30 years are Landsat-TM, Landsat-ETM+ continued by the new Landsat DCM, as well as NOAA-AVHRR data. Under cloud-free conditions the latter enables daily temperature monitoring of the earth's surface at a spatial resolution of 1.1 km reaching back to 1978, while the Landsat fleet enables observations at a higher resolution of 120 m (TM), 60 m (ETM+), and 100 m (LDCM) – although only at a 16 day revisit interval. The largest fleet of sensors supporting TIR research is currently operated by the USA, whereas the availability of European instruments monitoring the thermal domain has decreased in recent years due to the loss of the Envisat satellite (including the AATSR instrument). Currently, Europe acquires thermal data via the Meteosat satellites and is in the midst of preparing the launch of the Sentinel 3 mission with a thermal instrument on board. However, after the USA,

it is China which has the most operational thermal instruments in orbit. The Chinese fleet enabling temperature observations from 5 km down to 80 m spatial resolution in the TIR (CBERS-3) is foreseen to grow further. Data from these sensors hold a large potential for the thermal remote sensing community – especially if made more widely available internationally.

Acknowledgements The authors thank I. Schlegel and N. Lütge for checking the references. Further thanks go to two anonymous reviewers for valuable suggestions which helped to improve the manuscript.

References

- Abrams M, Hook SJ (1995) Simulated ASTER data for geologic studies. *IEEE Trans Geosci Remote Sens* 33(3):692–699
- Chen F, Tang L, Wang C, Qiu Q (2011) Recovering of the thermal band of Landsat 7 SLC-off ETM+ image using CBERS as auxiliary data. *Adv Space Res* 48(6):1086–1093
- European Space Agency, ESA (2012) The earth observation handbook: special edition for Rio +20. Available at: <http://www.eohandbook.com/>. Accessed Dec 2012
- Flynn LP, Harris AJL, Wright R (2001) Improved identification of volcanic features using Landsat 7 ETM+. *Remote Sens Environ* 78(2):180–193
- Kuenzer C (2005) Demarcating coal fire risk areas based on spectral test sequences and partial unmixing using multi sensor remote sensing data. Ph.D. thesis, Technical University Vienna, Vienna, 199pp
- Kuenzer C, Hecker C, Zhang J, Wessling S, Wagner W (2008) The potential of multi-diurnal MODIS thermal bands data for coal fire detection. *Int J Remote Sens* 29:923–944
- Mars JC, Rowan LC (2006) Regional mapping of phyllic- and argillic-altered rocks in Zagros magmatic arc, Iran, using advanced spaceborne thermal emission and reflection radiometer (ASTER) data and logical operator algorithms. *Geosphere* 2(3):161–186
- Pour AB, Hashim M (2012) The application of ASTER remote sensing data to porphyry copper and epithermal gold deposits. *Ore Geol Rev* 44:1–9
- Tangestani MH, Mazhari N, Agar B (2005) Mapping the porphyry copper alteration zones at the meiduk area, SE Iran, using the advanced spaceborne thermal emission and reflection radiometer (ASTER) data. In: Ehlers M, Michel U (eds) *Remote sensing for environmental monitoring, GIS applications, and geology*, vol 5983. SPIE, Brugge, p 59830
- Zhang J, Kuenzer C (2007) Thermal surface characteristics of coal fires 1: results of in-situ measurements. *J Appl Geophys* 63:117–134
- Zhang J, Kuenzer C, Tetzlaff A, Oettl D, Zhukov B, Wagner W (2007) Thermal characteristics of coal fires 2: results of measurements on simulated coal fires. *J Appl Geophys* 63:135–147